Otology & Neurotology
40:e150–e159 © 2018, Otology & Neurotology, Inc.

Linked-read Sequencing Analysis Reveals Tumor-specific Genome Variation Landscapes in Neurofibromatosis Type 2 (NF2) Patients

*Daniel S. Roberts, †Rahul Maurya, ‡§Yuka Takemon, ||Jeremie Vitte, †Liang Gong †Juanjuan Zhao, †Chee-Hong Wong, ¶William Slattery, ¶Kevin A. Peng, ¶Gregory Lekovic, **Marc S. Schwartz, *Ketan Bulsara, †Chew Yee Ngan, ||Marco Giovannini, and †Chia-Lin Wei

**School of Medicine, University of Connecticut; †The Jackson Laboratory for Genomic Medicine, Farmington, Connecticut; ‡The Jackson Laboratory, Bar Harbor; §Graduate School of Biomedical Science and Engineering, University of Maine, Orono, Maine; ||Department of Head and Neck Surgery, David Geffen School of Medicine at UCLA and Jonsson Comprehensive Cancer Center (JCCC), University of California, Los Angeles; ¶House Clinic and House Ear Institute, Los Angeles; and **University of California, San Diego, San Diego, California*

Hypothesis: We hypothesize that genomic variants including deletions, insertions, inversions, and tandem duplications beyond the changes in tumor suppressor *NF2* gene affect gene expression of tumor-specific pathways in vestibular schwannomas (VS) patients with Neurofibromatosis type 2 (NF2), thus contributing to their clinical behavior.
Background: Genomic variation could reconfigure transcription in NF2 transformation process. Therefore, genome-wide high-resolution characterization of structural variants (SV) landscapes in NF2 tumors can expand our understanding of the genes regulating the clinical phenotypes in NF2-associated VS.
Methods: We performed whole-genome haplotype-specific structural variation analysis using synthetic linked reads generated through microfluidics-based barcoding of high molecular weight DNA followed by high-coverage Illumina paired-end whole-genome sequencing from 10 patients' tumors of different growth rates and their matching blood samples.
Results: NF2 tumor-specific deletions and large SVs were detected and can be classified based on their association with tumor growth rates. Through detailed annotation of these mutations, we uncover common alleles affected by these deletions and large SVs that can be associated with signaling pathways implicated in cell proliferation and tumorigenesis.
Conclusion: The genomic variation landscape of NF2-related VS was investigated through whole-genome linked-read sequencing. Large SVs, in addition to deletions, were identified and may serve as modulators of clinical behavior. **Key Words:** Acoustic neuroma—Linked-read sequencing—NF2—Structural variants—Vestibular schwannoma.

Otol Neurotol **40:**e150–e159, 2019.

Vestibular schwannoma (VS) is the most common tumor of the cerebellopontine angle and arises from Schwann cells of vestibular nerves and is thought to result from mutations in the tumor suppressor *NF2/Merlin* gene. Neurofibromatosis type 2 (*NF2)* is located on chromosome 22 and regulates cell proliferation in response to adhesive signaling. Physiological roles include inhibition of signaling by integrins, receptor tyrosine kinases (1), and E3 ubiquitin ligase $CRL4^{DCAF1}$ activity (2).

NF2 is a dominantly inherited genetic disorder caused by germline or mosaic mutations in *NF2* (3) and characterized by bilateral VS, schwannomas of other cranial, spinal, and cutaneous nerves, meningiomas, and ependymomas. Patients with VS exhibit differential rates of growth and disease burden (4–6). The biology underlying these differences is relatively unknown.

The current understanding of tumorigenesis includes the presence of a mutation on a single allele of *NF2*, representing an initiating event in the development of disease. The loss of the remaining wild-type allele of *NF2*

Address correspondence and reprint requests to Daniel S. Roberts, M.D., Ph.D., 263 Farmington Avenue, Farmington, CT 06030; E-mail: droberts@uchc.edu; Chia-Lin Wei, Ph.D., 10 Discovery Drive, Farmington, CT 06032; E-mail: chia-lin.wei@jax.org

The content is solely the responsibility of the authors and does not necessarily represent the official views of the National Institutes of Health.

D.S.R and R.M. contributed equally to this work.

Y.T. and J.V. contributed equally to this work.

M.S.S., M.D., is a consultant and receives grant support from Cochlear Corporation for unrelated projects. Research reported in this publication was supported by the House Ear Institute and the National Cancer Institute of the National Institutes of Health under Award Number P30CA034196.

The authors disclose no conflicts of interest.

Supplemental digital content is available in the text.

DOI: 10.1097/MAO.0000000000002096

is reported to occur in the majority of patients with VS (7). However, the existence of additional driver mutations or structural variants (SVs) that may be important to tumor growth is unknown.

Genomic SV is prevalent in the human genome and the diversity of genome structure changes is associated with disease susceptibility (8–11). Many cancer genomes harbor significant SVs, and SVs are considered to be instrumental in promoting tumor progression (12,13). Detection of SVs can be used as the basis for tumor classification and predicting a therapeutic response (14,15). One recent study using next-generation sequencing strategies to survey the genomic landscape non-NF2 sporadic cranial and spinal schwannomas identified recurrent mutations at key regulatory genes (16). However, a comprehensive genetic analysis of NF2 has not been reported.

Short-read sequencing approaches have been widely used to study the abundance, diversity, and molecular features of SVs in human diseases (17,18). However, they lack the precision or resolution to decipher complex SV patterns or provide haplotype phasing of SVs in diploid genomes (19). Recently, long read sequencing approaches have emerged as promising avenues to delineate complex genome variations. Among them, linked long reads generated through barcoding long genomic DNA fragments in millions of micropartitions by microfluidics device coupled with high coverage massive parallel short-read sequencing technology enable the simultaneous characterization of a wide range of variations including single nucleotides, deletions, and complex SVs with phasing information (20,21).

In this study, we applied the linked long read approach to VS and matched blood samples for patients with the clinical diagnosis of NF2. We hypothesize that SVs beyond the expected single-nucleotide variations (SNVs) in *NF2* can act as the driver mutations that contribute to the variations in clinical behavior of VS in patients with NF2, defined by tumor growth rate. We detected thousands of SVs and provide the most extensive genomic resource in NF2 SV analysis to date.

METHODS

Specimens were obtained with institutional approval (Saint Vincent Medical Center, CA). Patients with high- and low-growth rates (five/each) were selected (high growth: $0.57 \pm 0.06\ cm^3$/mo versus low growth: $0.05 \pm - 0.02\ cm^3$/mo; $p = 0.0005$, paired t test) (Fig. 1, A and B). Groups were selected from a tumor bank of 75 tumors, and selection was based on the highest and lowest growth rates alone. Patients had not received radiation or bevacizumab treatment. Tumor growth rates were analyzed by calculating the volumetric growth between the last two magnetic resonance imaging scans before surgery. Volumetric estimations were performed using the ABC/2 (transverse × anterior-posterior × cranio-caudal)/2) (22). The average time between magnetic resonance imaging scans was 13.6 ± 3 SEM months. All tumor specimens had confirmed histopathology of VS. Epidemiological data were retrospectively collected (Table 1).

Sample Preparation for Linked-read Sequencing

DNA was extracted from the tumors and blood by MagAttract HMW DNA extraction kit (Qiagen, Hilden, Germany) and size-selected (>40 kb) on Pippin HT system (SAGE Science, Beverly, MA). 1 ng of HMW DNA input with roughly 300 copies of the human genome of 50 Kbp size was used as input for generating barcoded small fragments using the 10× Chromium and 10× Genomics (Pleasanton, CA). The instrument is a microfluidics droplet maker that can generate millions of emulsions of oil droplets. Each gel bead contains a functional oligo with a unique 16 bp barcode sequence and P5 adapter sequence. Within the emulsion, the gel bead disintegrates releasing the unique barcoded functional oligos and these oligos anneal randomly on the HMW DNA molecules thus generating unique barcoded fragments from the larger fragment by strand displacement amplification. All the amplified fragments arising from a single emulsion droplet have the same 16 bp barcodes (Fig. 1C). All the read pairs have the 16 bp unique barcode sequenced along with the insert read. All the reads with same barcode are called as linked reads. Libraries were prepared and sequenced 2 × 150 bp on Illumina X-TEN sequencer (Illumina, San Diego, CA) to 30× coverage.

Data Processing

All data were processed using Long Ranger v2.1.1. Data were demultiplexed using *longranger mkfastq* and alignment to hg19 human genome reference 10×_hg19_ucsc was performed using *Longranger wgs* (Fig. 1D).

Extracting Unique Phased SNVs

Unique variations from each sample were filtered by removing all common human variations, identified by dbSNP GRCh37p13 build 150, which were defined by a minor allele frequency of $>= 0.01$ using the Bedtools v.2.26.0 *intersect* operation on Long Ranger VCF output files (phased_variants.vcf.gz) (23). Tissue-specific SNVs focusing on *NF2* were further extracted also using this operation. The filtered phased VCF files were then read into the R statistical software v3.4.3 using R/Bioconductor package *vcfR* v3.6 for further analysis (24).

Identifying and Categorizing SNV Consequences for NF2

SNV that passed the Long Ranger filters were retained, and variant annotations and consequence predictions were performed using R/Bioconductor VariantAnnotate v3.6 with (UCSC references from R/Bioconductor TxDb.Hsapiens.UCSC.hg19.knownGene v3.6) (25,26). SNVs within *NF2* were categorized as frameshift, nonsense, nonsynonymous, and synonymous mutations (Table 2). Entrez gene identifiers produced during annotation were then decoded into HGNC symbols using R/Bioconductor org.Hs.eg.db v.3.6 (27).

Extracting and Annotating Deletion Calls

Tissue-specific and overlapping deletion calls (50–30,000 bp) were identified using R. Affected genes were annotated using R/Bioconductor package biomaRt v.2.6 (28).

Extracting and Annotating Tissue-specific Large SVs

Tissue-specific large SVs (>30 kb) were extracted using the bedtools *intersect* operation, followed by extraction of entries with passing filter in R. BiomaRt was used to interface with the Ensembl BioMart database genome build GRCh37, and each

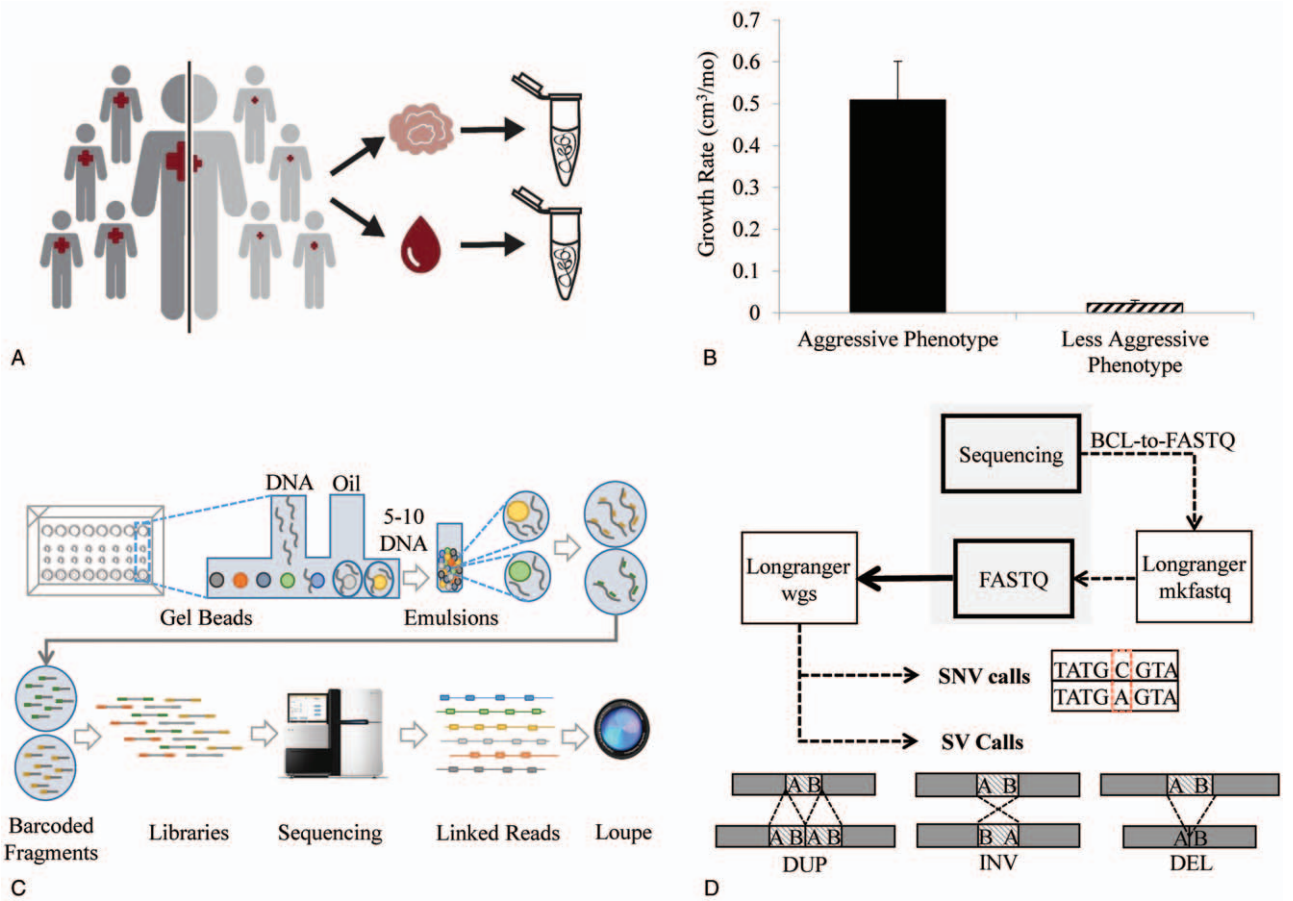

FIG. 1. Study workflow. *A,* The study comprises of five patients each from high-growth and low-growth rate patients groups. Matched blood and tumor samples were collected. *B,* Tumor Growth Rate of each phenotype. *C,* Linked-read sequencing workflow—HMW DNA with reagents, barcoded gel beads, and partitioning oil are loaded on a microfluidic chip on the instrument. Emulsion droplets are created, capturing 5 to 10 DNA strands in each gel bead. Strand displacement amplification takes place and all fragments arising from each droplet will have the same barcode. Standard library preparation steps are performed to add the sequencing adapter and sample index for sequencing. The blocks represent reads and the colored lines indicate linked reads of the same barcode. These linked reads were visualized in Loupe software. *D,* Data processing.

entry was annotated with HGNC symbols based on genome coordinates (27,28). Tissue-specific large SVs were further verified visually using the Loupe software.

Validation by PCR/qRT-PCR

Tumor-specific SVs were validated by PCR. Primers were designed to span breakpoints by Primer3 software to capture the SV breakpoint (primer sequences are shown in supplemental digital content 1, http://links.lww.com/MAO/A706) (29,30). 50 ng of HMW DNA extracted previously was used as input, forward and reverse primers were added along with hotstart PCR mastermix (KAPA Biosystems, Wilmington, MA). PCR amplification was performed by denaturing at 95 C for 3 minutes followed by 30 cycles of denature (98 C for 20 s) anneal (65 C for 15 s) and extension (72 C for 60 s) followed by final extension at 72 C for 5 minutes. Post PCR amplification, an Ampure bead clean-up step was performed and the samples were run on Agilent Tapestation to validate the size of the expected peaks.

Total RNA was extracted for gene expression analysis. The tumors were homogenized (Beadbug - Benchmark Scientific, Edison, NJ) and lysed in RLT buffer + 1% βME. RNA was extracted from the tumor lysate by Qiagen All Prep extraction kit (Qiagen, Germantown, MD). DNA contaminants were removed by performing a DNase treatment. Primers were designed to measure expression of *NF2*, *FBXW7,* together with three control genes *ACTB, B2 M*, and *RPL37A* (primer sequences are shown in supplemental digital content 1, http://links.lww.com/MAO/A706). *ACTB, B2 M*, and *RPL37A* were used as controls based on previous studies in similar tissue types (31–33). For each reaction, 50 ng of RNA input was taken and one-step qRT-PCR was performed by reverse transcription at 42 C for 5 minutes followed by incubation at 95 C for 3 minutes. Amplification was carried out at 95 C (3 s) and 60 C (20 s) for total of 40 cycles. Differential expression was calculated using the ddCT method.

RESULTS

Linked-read Sequencing of NF2 Patient Tumor and Blood Samples

Ten blood–tumor pairs with high or low tumor growth rates were selected based on growth rates alone (high

TABLE 1. *Clinical history of the patients selected*

Patient	Sex	Sporadic/ Familial	#1st Degree Relatives	Age	Growth Rate (cm^3/mo)	PTA	WR	Tumor Volume (cm^3)	Total CN Tumors	Cranial Meningioma	Spinal Meningioma	Ependymoma	Spinal Schwannoma
High-growth rate													
1	M	Sporadic	0	34	0.56	NR	NR	7.4	2	N	N	N	Y
2	M	Familial	1	23	0.44	NR	NR	12.1	5	N	N	N	Y
3	M	Familial	2	30	0.76	NR	NR	9.5	4	Y	N	N	Y
4	F	Sporadic	0	27	0.51	NR	NR	37.5	4	Y	Y	Y	Y
5	M	Sporadic	0	48	0.56	46	100	6.2	2	N	N	N	Y
Low-growth rate													
6	F	Familial	2	22	0.12	110	NR	1.4	3	Y	Y	N	Y
7	F	Sporadic	0	71	0.01	4	NR	0.7	2	N	N	N	N
8	F	Sporadic	0	32	0.04	NR	NR	2.1	3	N	N	N	N
9	F	Sporadic	0	63	0.03	23	88	7.4	2	N	N	N	N
10	F	Sporadic	0	50	0	83	8	1.3	2	N	N	N	N

CN indicates cranial nerve; NR, no response; PTA, pure-tone average; WR, word recognition.

growth: $0.57 \pm 0.06\,cm^3$/mo versus low growth: $0.05 \pm 0.02\,cm^3$/mo; $p = 0.0005$). Patient demographics are shown in Table 1. We generated barcoded libraries from the tumor and matched blood (Fig. 1). The mean sequencing coverage ranged 26.6× to 43.4×. The library quality and sequencing analysis are summarized (see table, Supplemental Digital Content 2, http://links.lww.com/MAO/A707). We achieved high-quality library datasets with high mapping rate with >99% of the genome coverage. Barcodes were distributed to more than 1.5 million individual DNA molecules. The average molecule length was from 24.7 to 102.4 Kbp with average 29 of N50 linked reads per molecule and megabase scale N50 phased block, which enabled efficient variant phasing. The phase blocks N50 detected ranged from 0.65 to 6.03 MB for all samples; the longest phase blocks detected ranged from 4.4 to 35.8 MB across 20 datasets (see table, Supplemental Digital Content 2, http://links.lww.com/MAO/A707).

Long Ranger (v2.1.1) pipeline also generates a list of SNVs focusing on *NF2* and genome-wide SVs. Three major types of variants were identified; SNVs with phasing information for *NF2* (see Table 2), deletions (50 bp−30 Kb), and large SVs (deletion, inversions, and duplication > 30 kbp). A list of all the high-confidence SVs detected is shown (see table, Supplemental Digital Content 3, http://links.lww.com/MAO/A708) and examples of these variants can be visualized in Figure 2. In

TABLE 2. *NF2 mutation status detected in each patient*

Patient	Sample Type	Chr	Start	End	Names	Ref	Var allele	Qual	Impact	REF CODON	VAR CODON	REF AA	VAR AA
Patient 1	T	chr22	30057302	30057302	chr22: 30057302_C/T	C	T	6.50E-05	Nonsense	CGA	TGA	R	*
Patient 2	T	chr22	30035110	30035110	chr22: 30035110_C/A	C	A	7.62E-11	Nonsynonymous	CCA	CAA	P	Q
Patient 2	T	chr22	30069280	30069281	chr22: 30069280_AC/A	AC	A	15.4993	Frameshift	GAC	GA		
Patient 2	B	chr22	30070880	30070880	chr22: 30070880_C/T	C	T	60.4988	Nonsense	CGA	TGA	R	*
Patient 4	T	chr22	30051652	30051652	chr22: 30051652_C/T	C	T	262.05	Nonsense	CGA	TGA	R	*
Patient 4	T	chr22	30057259	30057259	chr22: 30057259_G/A	G	A	1.47289	Synonymous	GAG	GAA	E	E
Patient 6	T	chr22	30038193	30038193	chr22: 30038193_A/T	A	T	0.08805	Synonymous	GTA	GTT	V	V
Patient 7	B	chr22	30067874	30067874	chr22: 30067874_G/A	G	A	4.84E-09	Synonymous	AGG	AGA	R	R
Patient 7	T AND B	chr22	30070880	30070880	chr22: 30070880_C/T	C	T	131.579	Nonsense	CGA	TGA	R	*
Patient 8	T	chr22	30050657	30050657	chr22: 30050657_C/G	C	G	45.793	Nonsense	TAC	TAG	Y	*
Patient 9	T	chr22	30032747	30032747	chr22: 30032747_G/A	G	A	2.07E-11	Nonsense	TGG	TAG	W	*
Patient 9	T	chr22	30069280	30069280	chr22: 30069280_A/T	A	T	2.42481	Nonsynonymous	GAC	GTC	D	V
Patient 9	B	chr22	30077584	30077584	chr22: 30077584_T/TA	T	TA	9.19E-15	Frameshift	ATT	ATTA		
Patient 10	T	chr22	30050656	30050657	chr22: 30050656_AC/A	AC	A	19.844	Frameshift	TAC	TA		

SAMPLE TYPE: T indicates tumor; B, blood; T AND B, both (tumor and blood).
QUAL field is an estimate of the barcode support for the corresponding event. A call with QUAL score >15 is a high confidence call.
VAR AA: * refers to STOP Codon.

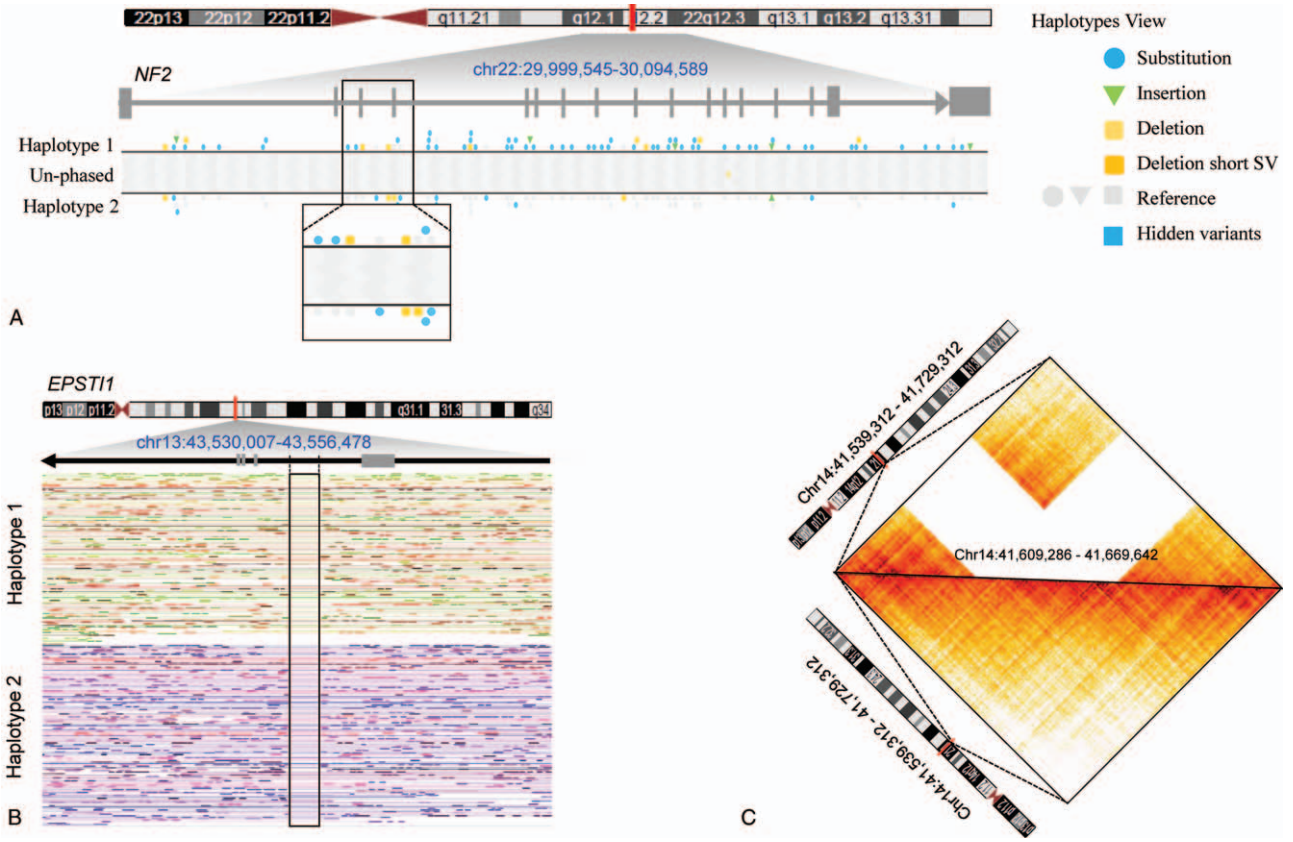

FIG. 2. Different types of variants detected by linked-read analysis visualized in the Loupe browser. *A,* SNVs in the *NF2* gene region (chr22:29,999,545–30,094,589). Top: chromosome 22 ideogram with *NF2* gene region highlighted followed by the zoom-in view of the *NF2* gene structure in parallel of the SNVs/small deletion detected in each haplotype in two separate phased tracks. Different types of SNVs are represented by different color symbols. The 3rd and 4th exon regions are zoom in to show the detailed substitutions (blue) and deletions (orange). A homozygous SNV would be present only on both the haplotypes while a heterozygous SNV would be present in just one haplotype. *B,* 1.6 Kb deletion in the *EPSTI1* intronic region. Chromosome 13 ideogram with *EPSTI1* gene region highlighted is shown above followed by a zoom-in view of the partial coding exons-introns (chr13:43,530,007-43,556,478). Linked reads spanned in this region are shown in two separated phased tracks as either orange-yellow color reads (haplotype 1) and pink-purple read (haplotype 2). A 1.6 Kb homozygous deletion in the intronic region in chr13: 43539796–43541448 is shown (box) where no linked reads were found. *C,* A 60 Kb large deletion found in patient #2 The heatmap of the linked-read distribution across chr14:41,539,312 - 41,729,312 (coordinates on the *x* and *y* axes). The deletion is shown as a blank region with no aligned reads in the matrix view from the patient two tumor sample (top panel) in comparison with control from patient seven (lower panel).

total, we uncovered 10 to 18 somatic large SVs in tumor samples and 13 to 22 germline large SVs in their corresponding matching blood, respectively. The total numbers of deletion calls were from 3,720 to 4,894 between NF2 tumors and their matching blood samples.

Haplotype-specific Single Nucleotide NF2 Mutations Uncovered in Tumors

We examined the SNV profiles in *NF2*. Previous studies suggest that mutation of a single allele of *NF2* should be present and that the loss of the remaining wild-type allele of *NF2* is reported to occur in the preponderance of patients. The dbSNP filtered SNVs for all the samples in the *NF2* gene region were identified as synonymous, nonsynonymous, frameshift, or nonsense mutations based on their impact in coding sequences (Table 2). We identified tumor-specific SNVs in 7 out of 10 patients and 6 of them are either nonsense or frameshift mutations. Expression of *NF2* was reduced in patients 2 and 10 where frameshifts were detected in *NF2* genes (Fig. 3B), suggesting that the consequences of these frameshift mutations may affect *NF2* transcripts. Interestingly, the expression trended toward lower levels in the high-growth tumors ($p = 0.11$) (Fig. 3A), supporting the role of *NF2* dysregulation in the high-growth phenotype.

Deletions (50 bp to 30 Kbp) Detected in NF2 Tumors

We focused on deletions between 50 bp to 30 Kbp in each patient and compared them across tumor and blood samples. We detected ~5K to 6K deletions in each patient and ~ 29% were only found in tumor samples while majority of them were common between tumor and matching blood (see table, Supplemental Digital Content 4, http://links.lww.com/MAO/A709). Figure 3C represents the distribution of these deletion calls from each

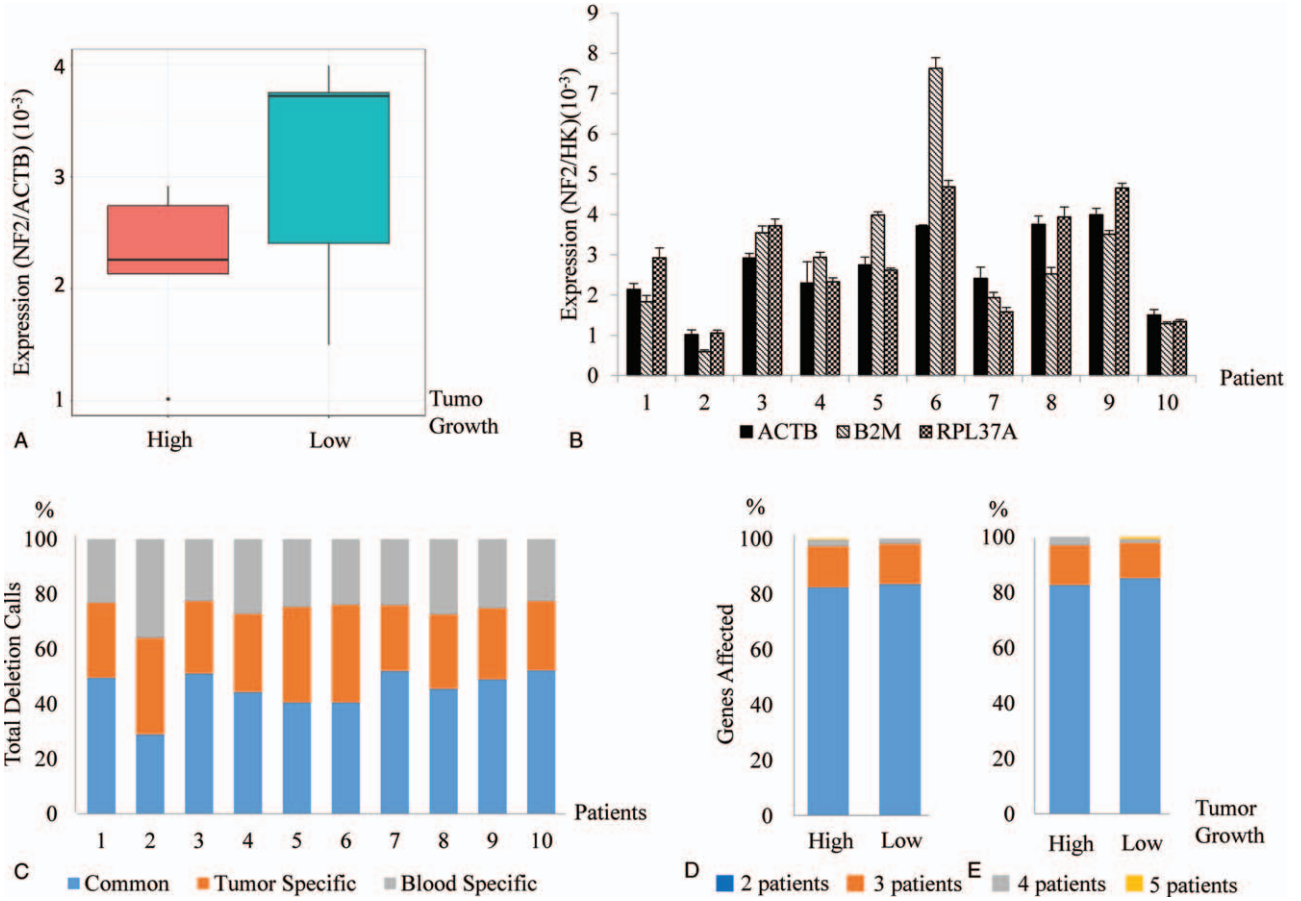

FIG. 3. *A,* Comparison of *NF2* gene expression normalized to *ACTB* in the high-growth and low-growth tumor groups. *B,* Analysis of *NF2* gene expression by qRT-PCR by normalizing to three housekeeping genes as controls (*ACTB*, *B2M,* and *RPL37A*) in each patient. *C,* Deletion Calls Comparison—Distribution and comparison of the deletion calls (50 bp–30 Kbp) across patients. *D,* Somatic deletion calls affecting genes—Distribution of the affected somatic deletions (tumor only) shared between two or more patients. *E,* Germline deletion calls affecting genes—Distribution of the affected germline deletions (blood and common) shared between two or more patients.

patient. When we examined between the 587 and 1,260 genes affected by these deletions only detected in tumor, vast majority were within gene regions; demonstrating an enrichment of deletions affected gene expression. A total of 2,928 genes were affected by the 3,880 tumor associated deletions in the high-growth tumors and 2,781 genes were interrupted by the 3,586 deletions associated with slow-growth tumor type. Among them, 298 and 208 genes were identified in multiple patients with high- and low-growth categories, respectively (Fig. 3D). The relative frequencies of shared genes between the two groups are listed (see table, Supplemental Digital Content 5, http://links.lww.com/MAO/A710). When focusing on common genes to the high-growth tumor group, 7 genes were commonly found in at least 4/5 high-growth tumor patients (*NPIPP1, PDXDC1, RASGEF1B, TTC34, VEGFC, WDR27, ZEB2*) and 1 target was present in 5/5 high-growth tumors (*TSPAN8)*. We focused on target genes that may be important to NF2 based on known literature. VEGFC and TSPAN have putative roles in the regulation of VEGFA signaling and cell adhesion/ angiogenesis respectively.

Recent data suggest the possibility for important recurrent mutations in sporadic VS in several chromatin remodeling genes (*ARID1A, ARID1B*) and *DDR1* which is a gene encoding a receptor tyrosine kinase (16). Notably, deletions in *ARID1A* were identified in one patient and deletions in *ARID1B* were identified in two patients. Similarly, we detected genes affected by germline deletions which could influence the growth rate of NF2 tumors. Among these germline deletions, 133 and 142 genes were identified in multiple patients with high- and low-growth categories, respectively (Fig. 3E). The relative frequencies of shared genes between the two groups are listed (see table, Supplemental Digital Content 5, http://links.lww.com/MAO/A710).

Large SVs Detected in NF2 Patients

SVs were identified by deviations in barcode coverage which is a method unique to linked-read sequencing (34). Fourteen to 27 large SVs were detected in each patient (see table, Supplemental Digital Content 6, http://links.lww.com/MAO/A711). Tumor-specific SVs were identified bioinformatically and then visually verified using

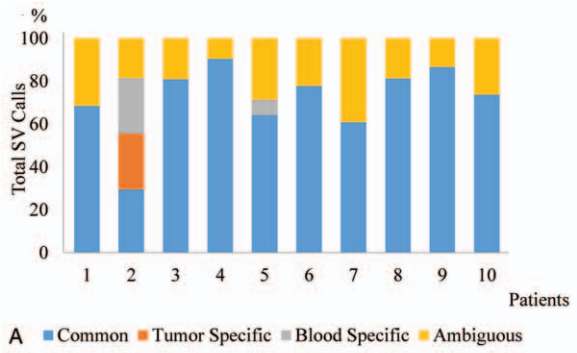

CHROM	START POS	END POS	SVTYPE	SPAN	QUAL	GENES
chr2	34695839	34736558	DEL	40,719	102	NA
chr3*	129763391	129806736	DEL	43,345	65	*ALG1L2*
chr4	153228982	153341306	DUP	112,324	37	*FBXW7*
chr13	57752480	57788855	DEL	36,375	47	NA
chr14	41609313	41669653	DEL	60,340	259	NA
chr16	34401028	34450085	INV	49,057	50	NA
chr22	29948106	30014910	DEL	66,804	33	*THOC5, NIPSNAP1, NF2*

B

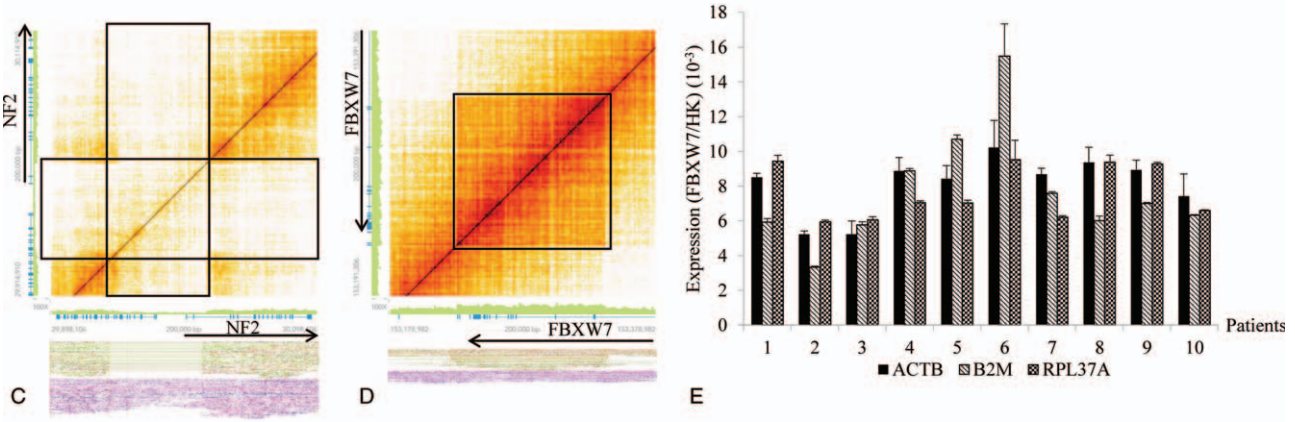

FIG. 4. SV Calls Comparison. *A,* Distribution and comparison of the large SV calls (>30 Kb) across all patients. *B*, Tumor-specific SV calls in Patient 2. *Similar large SV and SVTYPE in tumor-normal pair of the same patient but tumor SV is heterozygous and blood SV is homozygous. *C,* A 66 Kb heterozygous deletion on Chr22 spanning over the 5' end of the NF2 gene of Patient 2 tumor sample. (Top) The heatmap with same chromosome coordinates on *x* and *y* axes and the large black blocks indicate the region of heterozygous deletion. (Bottom) Linked reads for each haplotype. A deletion is clearly observed in the first haplotype (orange-green color). *D,* Inversion in Chr 4—a 112Kb tandem duplication on Chr4, spanning over the FBXW7, a known tumor suppressor gene. (Top) The heatmap where the black block indicates the region of tandem duplication. (Bottom) Multiple linked reads aligning to the duplicated region. *E, FBXW7* gene expression (by qRT-PCR) normalized to three housekeeping genes as controls (*ACTB*, *B2M* and *RPL37A)* across all patients.

Loupe by examining regions harboring large SVs called in tumor samples and/or their matched blood data. Any SV that could not be assigned to either tumor or blood group was classified as ambiguous. A list of all the SVs only found in either tumor or blood was compiled (see table, Supplemental Digital Content 6, http://links.lww.com/MAO/A711). The distribution of the SVs in each of the categories across 10 patients is illustrated in Figure 4A. The tumor sample in patient #2 contained the most (7) tumor-specific SVs (Fig. 4B). One large heterozygous 66 Kbp deletion spanned the 5' end of the *NF2* gene (Fig. 4C) and a large tandem duplication of 112 Kbp which disrupts the 3' exons of a known tumor suppressor, F-box protein, and WD repeat containing protein 7 (FBXW7) on chromosome 4 (Fig. 4D). To evaluate the impact of the SVs on their affected genes, expression of *NF2* and *FBXW7* was determined in tumor cells from all 10 patients. Both genes showed reduced expression in patient 2 (Figs. 3B and 4E). FBXW7 is a known tumor suppressor and its loss of function has been linked to uncontrolled centriole duplication and hepatocellular carcinoma (35,36). FBXW7's role in regulating cell cycle and proliferation makes it a candidate for exacerbating the NF2 disease progression in the high-growth subgroup.

Expression of data for sporadic schwannomas indicates a 10% rate of SH3PXD2A-HTRA1 fusion proteins and sporadic schwannomas as the consequence of a balanced 19-Mb chromosomal inversion on chromosome 10q (16). In our analysis of 10 tumors, no balanced translocations resulting in a *SH3PXD2A-HTRA1* fusion were identified.

DISCUSSION

Next-generation DNA sequencing technologies provide the opportunity to broaden our understanding of genetic aberrations beyond SNV, through technological advancement, and to now consider specific SVs that may contribute to disease phenotype. Long-read sequencing technology allows for high-resolution analysis of SV at the genome-wide level, and is able to capture complex rearrangements. Here, we leverage the recent technology advancement in microfluidics-based linked reads analysis to identify different types of SVs. Our results demonstrate that this approach is effective to capture large numbers deletions and SVs in the NF2 patient population.

While the importance of SV is considered for oncogenic tumorigenesis, a role for SV has not been fully considered for patients with NF2 (37). Importantly, in addition to the expected SNV within *NF2*, we identified tumor-specific deletions and large SVs. SVs were present at seven loci in one patient with an aggressive phenotype including a deletion in *NF2* and a duplication in *FBXW7*.

The contribution of large SV to the phenotype is not well understood. Studies to date concentrated on *NF2* loci alone. In a study of 54 causative *NF2* mutations, Evans et al., through PCR amplification of genomic DNA at NF2, identified five large deletions ranging from 650 to 5 kb. The remaining mutations were SNVs leading to frameshift, missense, splice site mutations. Patients with truncating mutations were more likely to have severe disease phenotype including growth rate (38). While the SV including *NF2* seems to be an important finding, it is unknown whether SVs at other loci are important for phenotype.

In a rapidly growing VS, we identified a large SV the included *FBXW7*. FBXW7 is a subunit of an ubiquitin ligase that targets proteins for degradation. The SV was a tandem duplication affecting exon 2 through 13, out of 13 exons and disruption in expression is predicted by this change. *FBXW7* is strongly associated with tumorigenesis in a multitude of human cancer (35) and is a regulator of ubiquitin-mediated degradation of cyclin E, c-Myc, c-Jun, Notch, Mcl-1, and mTOR (39,40). The finding of a large SV at *FBXW7* is an intriguing finding. Data suggest a role for inhibition rapamycin complex 1 (mTORC1) as a therapeutic approach for NF2. The functional loss of merlin associated with NF2 results in elevated mTORC1 signaling in NF2-related tumors (41) and clinical trials show promise for tumor growth stabilization by directly targeting mTORC1 (42). Data suggest that *FBXW7* plays a critical role in limiting mTOR function in the developmental regulation of myelination (43), suggesting that SV at *FBXW7* could influence tumor growth in VS.

Possibly, the most important finding of our study is the presence of recurrent deletions, repeated in tumors with high-growth rates. Among these deletions, 5/5 patients shared tumor-specific deletions TSPAN and 4/5 shared VEGFC. TSPAN8 expression occurs in several malignancies including esophageal cancer (44) and mechanistically is thought to modulate cell adhesion and angiogenesis (45). Levels of expression in VS are unknown and a role in the pathogenesis of NF2 will need to be investigated further. VEGF-associated proteins have received attention because the anti-VEGF antibody bevacizumab specifically target VEGFA, and treatment of NF2-associated VS with bevacizumab led to a volumetric decrease in 55% of VSs and improved speech perception in some patients (46,47). VEGFC is an alternative ligand to VEGF-A for VEGFR-2 binding, which is thought to promote tumor angiogenesis. The complex interplay between these factors is not known in VS and the consequences of a deletion of *VEGFC* will need to be evaluated. However, a meta-analysis of six randomized phase III trials in colorectal, pancreatic, lung, renal, breast, and gastric cancer suggests a possible role for *VEGFC* (48). Within this study, genetic variance of *VEGFC* was predictive of bevacizumab treatment response across tumor types suggesting the possible importance for our findings.

We demonstrated that 8 of 10 patients had at least 1 mutation at *NF2* in either tumor or matching blood and 4 patients had 2 or more mutations. These findings are consistent with a larger study focusing on schwannomas from patients with NF2 where one mutation was presents in (86/97) 89% and two mutations were present in (13/97) 13% specimens (49). These data are also comparable to non-NF2 VS where exome sequencing analysis showed (35/46) 76% tumors harbored mutations in *NF2* and 16 tumors (35%) had 2 mutational events (50). Next-generation sequencing was recently used for studying the genomic landscape of schwannomas in non-NF2 cases. Agnihotri et al. (16) in 2016 performed whole-exome sequencing on 13 sporadic cranial and 13 sporadic spinal schwannomas. *NF2* was altered either by mutation or 22q loss in (20/26) 77% of patients consistent with our findings suggesting similarities between NF2 and non-NF2 VS.

Our findings indicate that recurrent deletions were present at *ARID1A*, *ARID1B* in a subset of patients. *ARID1* proteins regulate chromatin remodeling through the recruitment of transcriptional activators or repressors (51,52). Recurrent deletions at *ARID1A*, *ARID1B* in a subset of tumor and blood specimens suggest possible similarities between sporadic VS and tumors associated with NF2.

RNA sequencing previously identified an in-frame SH3PXD2A-HTRA1 fusion in 10% of 125 samples analyzed, and in vitro studies showed that stable expression of this fusion protein promoted growth in the HEI-193 immortalized schwannoma cells (16). An important question is whether these changes, identified for non-NF2 schwannoma, are also found in NF2. Large SV, consistent with the SH3PXD2A-HTRA1 fusion, were not present in our study. These findings suggest that the genomic landscape of NF2 differs from sporadic schwannomas.

Understanding the comprehensive genetic landscape of NF2 has not been performed to date through genome-wide sequencing efforts. Our pilot study suggests a role for this approach to identify additional targets that may influence tumor growth. We have identified large SVs, and common recurrent deletions shared among tumors with high growth with rates in those with low-growth rates. The limitations of our study are most notably sample size, with a larger study planned. However, despite this limitation, we demonstrate the utility of next-generation DNA sequencing technologies to identify recurrent shared variance in our patient cohort. Such an approach has catalyzed new gene targets for clinical drug trials and suggests a possible role for personalized therapeutic approaches, based on whole-genome analysis for NF2 (53–55). These directed translational approaches are advocated by the NF2 research

community as an important resource to facilitate new treatments for patients with NF2 (56).

Acknowledgments: The authors thank Dr. Alyssa Lau for efforts in illustrating the figures.

REFERENCES

1. Cooper J, Giancotti FG. Molecular insights into NF2/Merlin tumor suppressor function. *FEBS Lett* 2014;588:2743–52.
2. Li W, You L, Cooper J, et al. Merlin/NF2 suppresses tumorigenesis by inhibiting the E3 ubiquitin ligase CRL4(DCAF1) in the nucleus. *Cell* 2010;140:477–90.
3. Trofatter JA, MacCollin MM, Rutter JL, et al. A novel moesin-, ezrin-, radixin-like gene is a candidate for the neurofibromatosis 2 tumor suppressor. *Cell* 1993;72:791–800.
4. Hoa M, Slattery WH 3rd. Neurofibromatosis 2. *Otolaryngol Clin North Am* 2012;45:315–32.
5. Stangerup SE, Caye-Thomasen P. Epidemiology and natural history of vestibular schwannomas. *Otolaryngol Clin North Am* 2012;45:257–68.
6. Plotkin SR, Merker VL, Muzikansky A, et al. Natural history of vestibular schwannoma growth and hearing decline in newly diagnosed neurofibromatosis type 2 patients. *Otol Neurotol* 2014;35: e50–6.
7. Selvanathan SK, Shenton A, Ferner R, et al. Further genotype—phenotype correlations in neurofibromatosis 2. *Clin Genet* 2010;77:163–70.
8. Mehrian-Shai R, Freedman S, Shams S, et al. Schwannomas exhibit distinct size-dependent gene-expression patterns. *Future Oncol* 2015;11:1751–8.
9. Sudmant PH, Rausch T, Gardner EJ, et al. An integrated map of structural variation in 2,504 human genomes. *Nature* 2015;526: 75–81.
10. Weischenfeldt J, Symmons O, Spitz F, et al. Phenotypic impact of genomic structural variation: Insights from and for human disease. *Nat Rev Genet* 2013;14:125–38.
11. Conrad DF, Pinto D, Redon R, et al. Origins and functional impact of copy number variation in the human genome. *Nature* 2010;464:704–12.
12. Stankiewicz P1, Lupski JR. Structural variation in the human genome and its role in disease. *Annu Rev Med* 2010;61:437–55.
13. Diskin SJ, Hou C, Glessner JT, et al. Copy number variation at 1q21.1 associated with neuroblastoma. *Nature* 2009;459:987–91.
14. Edwards PA. Fusion genes and chromosome translocations in the common epithelial cancers. *J Pathol* 2010;220:244–54.
15. Menghi F, Inaki K, Woo X, et al. The tandem duplicator phenotype as a distinct genomic configuration in cancer. *Proc Natl Acad Sci U S A* 2016;113:E2373–82.
16. Agnihotri S, Jalali S, Wilson MR, et al. The genomic landscape of schwannoma. *Nat Genet* 2016;48:1339–48.
17. Auton A, Brooks LD, Durbin RM, et al., 1000 Genomes Project Consortium. A global reference for human genetic variation. *Nature* 2015;526:68–74.
18. Chen X, Schulz-Trieglaff O, Shaw R, et al. Manta: Rapid detection of structural variants and indels for germline and cancer sequencing applications. *Bioinformatics* 2016;32:1220–2.
19. Ye K, Schulz MH, Long Q, et al. Pindel: A pattern growth approach to detect break points of large deletions and medium sized insertions from paired-end short reads. *Bioinformatics* 2009;25:2865–71.
20. Chaisson MJ, Wilson RK, Eichler EE. Genetic variation and the de novo assembly of human genomes. *Nat Rev Genet* 2015;16:627–40.
21. Zheng GX, Lau BT, Schnall-Levin M, et al. Haplotyping germline and cancer genomes with high-throughput linked-read sequencing. *Nat Biotechnol* 2016;34:303–11.
22. Bathla G, Policeni B, Hansen MR, Berbaum K. Calculating the tumor volumes in vestibular schwannomas: Are the ABC/2 and volumetric methods comparable? *Otol Neurotol* 2017;38:889–94.
23. Quinlan AR, Hall IM. BEDTools: A flexible suite of utilities for comparing genomic features. *Bioinformatics* 2010;26:841–2.
24. Knaus BJ, Grünwald NJ. VCFR: A package to manipulate and visualize variant call format data in R. *Mol Ecol Resour* 2017;17:44–53.
25. Obenchain V, Lawrence M, Carey V, et al. VariantAnnotation: A Bioconductor package for exploration and annotation of genetic variants. *Bioinformatics* 2014;30:2076–8.
26. Carlson M and Maintainer BP (2015). TxDb.Hsapiens.UCSC.hg19.knownGene: Annotation package for TxDb object(s). R package version 3.2.2.
27. Carlson M (2017). org.Hs.eg.db: Genome wide annotation for Human. R package version 3.5.0.
28. Durinck S, Spellman P, Birney E, Huber W. Mapping identifiers for the integration of genomic datasets with the R/Bioconductor package biomaRt. *Nat Protoc* 2009;4:1184–91.
29. Koressaar T, Remm M. Enhancements and modifications of primer design program Primer3. *Bioinformatics* 2007;23:1289–91.
30. Untergasser A, Cutcutache I, Koressaar T, et al. Primer3—new capabilities and interfaces. *Nucleic Acids Res* 2012;40:e115.
31. Pfister C, Tatabiga MS, Roser F. Selection of suitable reference genes for quantitative real-time polymerase chain reaction in human meningiomas and arachnoidea. *BMC Res Notes* 2011;4:275.
32. Liu Z, Jin YQ, Chen L, et al. Specific marker expression and cell state of Schwann cells during culture in vitro. *PLoS One* 2015;10:e0123278.
33. Colciago A, Melfi S, Giannotti G, et al. Tumor suppressor Nf2/merlin drives Schwann cell changes following electromagnetic field exposure through Hippo-dependent mechanisms. *Cell Death Discov* 2015;1:15021.
34. Obenchain V, Lawrence M, Carey V, et al. VariantAnnotation: A bioconductor package for exploration and annotation of genetic variants. *Bioinformatics* 2014;30:2076–8.
35. Cao J, Ge MH, Ling ZQ. Fbxw7 tumor suppressor: A vital regulator contributes to human tumorigenesis. *Medicine (Baltimore)* 2016;95:e2496.
36. Zhou Z, He C, Wang J. Regulation mechanism of Fbxw7-related signaling pathways (Review). *Oncol Rep* 2015;34:2215–24.
37. Wrzeszczynski K, Felice V, Shah M, et al. Whole genome sequencing-based discovery of structural variants in glioblastoma. *Methods Mol Biol* 2018;1741:1–29.
38. Hexter A, Jones A, Joe H, et al., English Specialist NF2 Research Group. Clinical and molecular predictors of mortality in neurofibromatosis 2: A UK national analysis of 1192 patients. *J Med Genet* 2015;52:699–705.
39. Cizmecioglu O, Krause A, Bahtz R, et al. Plk2 regulates centriole duplication through phosphorylation-mediated degradation of Fbxw7 (human Cdc4). *J Cell Sci* 2012;125 (pt 4):981–92.
40. Zhou Z, He C, Wang J1. Regulation mechanism of Fbxw7-related signaling pathways (Review). *Oncol Rep* 2015;34:2215–24.
41. Giovannini M, Bonne NX, Vitte J, et al. mTORC1 inhibition delays growth of neurofibromatosis type 2 schwannoma. *Neuro Oncol* 2014;16:493–504.
42. Goutagny S, Raymond E, Esposito-Farese M, et al. Phase II study of mTORC1 inhibition by everolimus in neurofibromatosis type 2 patients with growing vestibular schwannomas. *J Neurooncol* 2015;122:313–20.
43. Kearns CA, Ravanelli AM, Cooper K, et al. Fbxw7 Limits Myelination by Inhibiting mTOR Signaling. *J Neurosci* 2015;35:14861–7.
44. Zhou Z, Ran YL, Hu H, et al. TM4SF3 promotes esophageal carcinoma metastasis via upregulating ADAM12m expression. *Clin Exp Metastasis* 2008;25:537–48.
45. Maisonial-Besset A, Witkowski T, Navarro-Teulon I, et al. Tetraspanin 8 (TSPAN 8) as a potential target for radio-immunotherapy of colorectal cancer. *Oncotarget* 2017;8:22034–47.
46. Plotkin SR, Stemmer-Rachamimov AO, Barker FG 2nd, et al. Hearing improvement after bevacizumab in patients with neurofibromatosis type 2. *N Engl J Med.* 2009;361:358–67.
47. Plotkin SR, Merker VL, Halpin C, et al. Bevacizumab for progressive vestibular schwannoma in neurofibromatosis type 2: A retrospective review of 31 patients. *Otol Neurotol* 2012;33:1046–52.

48. de Haas S, Delmar P, Bansal AT, et al. Genetic variability of VEGF pathway genes in six randomized phase III trials assessing the addition of bevacizumab to standard therapy. *Angiogenesis* 2014;17:909–20.
49. Hadfield KD, Smith MJ, Urquhart JE, et al. Rates of loss of heterozygosity and mitotic recombination in NF2 schwannomas, sporadic vestibular schwannomas and schwannomatosis schwannomas. *Oncogene* 2010;29:6216–21.
50. Håvik AL, Bruland O, Myrseth E, et al. Genetic landscape of sporadic vestibular schwannoma. *J Neurosurg* 2018;128: 911–22.
51. Dallas PB, Cheney IW, Liao DW, et al. p300/CREB binding protein-related protein p270 is a component of mammalian SWI/SNF complexes. *Mol Cell Biol* 1998;18:3596–603.
52. Nie Z, Xue Y, Yang D, et al. A specificity and targeting subunit of a human SWI/SNF family-related chromatin-remodeling complex. *Mol Cell Biol* 2000;20:8879–88.
53. Siu LL, Conley BA, Boerner S, et al. Next-generation sequencing to guide clinical trials. *Clin Cancer Res* 2015;21:4536–44.
54. Biesecker LG, Green RC. Diagnostic clinical genome and exome sequencing. *N Engl J Med* 2014;370:2418–25.
55. Craig DW, O'Shaughnessy JA, Kiefer JA, et al. Genome and transcriptome sequencing in prospective metastatic triple-negative breast cancer uncovers therapeutic vulnerabilities. *Mol Cancer Ther* 2013;12:104–16.
56. Blakeley JO, Evans DG, Adler J, et al. Consensus recommendations for current treatments and accelerating clinical trials for patients with neurofibromatosis type 2. *Am J Med Genet A* 2012;158A:24–41.